Original Article

Institution of MECHANICAL ENGINEERS
Journal of MECHANICAL ENGINEERING SCIENCE

# Slant type taper profiling and prediction of profiling speed for a circular profile during in wire electric discharge machining using Hastelloy-X

Proc IMechE Part C:
J Mechanical Engineering Science
2021, Vol. 235(21) 5511–5524

DOI: 10.1177/0954406221992398
journals.sagepub.com/home/pic
SAGE

**IV Manoj and S Narendranath**

## Abstract

Hastelloy-X a nickel-based alloy used in nozzles, flame holders, turbine blades, turbocharges, jet engine tailpipes, afterburner components etc. having complex tapering profiles. Wire electric discharge machining proves to be the most beneficial machining technique as it provides required accuracy for the components. In the present research, a slant type taper fixture is employed for achieving taper angles as convention tapering have many hindrances like wire bend, angular inaccuracy, guide wear, insufficient flushing and wire breakage etc. and machining a simple circular profile on Hastelloy-X. The behaviour of different output parameters like profiling speed, surface roughness, profile areas, microhardness and recast layer were investigated for various input parameters for machined taper components at 0°, 15° and 30°. The cutting speed override parameter influenced most on the profiling speed and surface roughness. The wire offset parameter was found to be the most significant factor in the case of circular profile areas that were machined. The variation of different output parameters to profiling/cutting speed and taper angle was also highlighted. It is found the recast layer decreased which indicated lesser thermal degradation at higher taper angles at different profiling parameters. This is also validated by the microhardness where the machined surface hardness of taper angular profiles was found to be greater than the 0° profiles. The artificial neural networks and adaptive neuro-fuzzy interference system were used for the prediction of profiling speed. The adaptive neuro-fuzzy interference system was found better in prediction as the percentage error varies between 0–5 per cent. In conclusion, the profiling speed influences both on the accuracy and surface of machined taper circular profiles.

## Keywords

WEDM tapering, slant type taper fixture, profiling speed, circular area, artificial neural networks and adaptive neuro-fuzzy interference system.

Date received: 31 October 2020; accepted: 15 January 2021

## Introduction

Nickel-based superalloys are high-temperature resistant alloys having various applications in jet engines, gas turbines and rocket applications due to their mechanical properties.[1,2] Hastelloy-X a nickel-chromium-iron-molybdenum alloy used in many industries such as aerospace, marine, chemical, nuclear, mould and stamping industries etc. The property of high-temperature strength and low thermal diffusivity poses a challenge for machining such superalloys.[3] Wire electric discharge machining (WEDM) a non-conventional and non-contact technique have gained prominence as it can machine various materials like nickel, titanium alloys, die and tool steels, composites etc.[4–6] The complexity in applications advocates taper/oblique machining in WEDM as it become a requirement. Many researchers have identified the disadvantages during taper/oblique machining in WEDM like angular inaccuracies, bending of wire, wire breakage, guide wear and friction, incomplete flushing, etc.[7–9] Researchers like Yan et al.,[10] Martowibowo and Wahyudi[11] and Manoj et al.[12,13] have incorporated innovative methods to avoid drawbacks of the tapering process in WEDM by introducing new guide fixtures, material and mechanisms.

Department of Mechanical Engineering, National Institute of Technology Karnataka, Surathkal, India

**Corresponding author:**
IV Manoj, Department of Mechanical Engineering, National Institute of Technology Karnataka, Surathkal 575025, India.
Email: vishalmanojvs@gmail.com

Gong et al.[14] have reported that the electrical parameters like peak current had the greatest effect than non-electrical parameters on surface roughness and machining time. Tahir and Jahanzaib[15] have conducted WEDM of high-strength low-alloy by both cold treatment and non-cold treated brass wires. It was found that pulse on time was the most contributing factor on cutting speed, surface roughness and kerf. Khatri and Rathod.[16] have explored the WEDM of thin sheets of titanium alloy by the concentric flow of gaseous dielectric fluid in which it was found that dielectric fluid leads to 18% faster-cutting cycles, 7% reduced kerf width and 10% improved MRR. Firouzabadi and Parvizian[17] have highlighted machining and restoring curved corners of small-radius convex and concave corner radii errors by successive cutting. Dodun et al.[18] have reported WEDM of thin parts of aluminium and steel. Its behaviour of bending of crest due to the magnetic property of workpiece.

The most common method of ANN and ANFIS was adopted for prediction of profiling speed. Jafari et al.[19] have predicted the surface roughness parameters using artificial neural networks (ANN) in micro-WEDM of copper. It was found the predicted values were in very good agreement with the coefficient of determination of 99.5%. Azhiri et al.[20] employed an adaptive neuro-fuzzy inference system (ANFIS) model could predict and study the relation of the cutting velocity and surface roughness in WEDM of Al/SiC metal matrix composite. Naresh et al.[21] have investigated different aspects of ANN and ANFIS models for better prediction of material removal rate and surface roughness. It was concluded that the ANFIS model with gaussian membership function was the best model amongst all ANN and ANFIS models employed.

From the literature survey, we can observe that profiling/cutting speed is a vital parameter in machining. The angle considered for studies was varied from 0° to 30° angles due to the applications and workpiece thickness. In the present study, taper circular profiles were WEDMed using an innovative slant type taper fixture on Hastelloy-X. This method enabled to machine tapered profiles of desired angles avoiding the disadvantage of conventional machining. Different machining performance characteristic features like profiling speed, surface roughness, profile areas, microhardness and recast layer during tapering. The input parameters like wire guide distance ($\vartheta$), corner dwell time ($\mu$), wire offset ($\varphi$) and cutting speed override ($\omega$) were utilized to get tapered components. Taguchi's $L_{16}$ array was used at all the three angles and it was also found that the taper angle also influenced different response parameters. The profiling speed and surface roughness were found to be influenced mainly by $\omega$ parameter. The effect of input parameters on taper circular profile areas was highlighted. The variation in microhardness and recast layer were investigated at various taper angles for highest and lowest parameters. The profiling speed that proved to be an essential factor was predicted using ANN and ANFIS system for various input parameters at different taper angles.

## Workpiece and experimental strategy

### Workpiece

Hastelloy-X alloy is a combination of nickel-chromium-iron-molybdenum alloy also called as alloy-X. Alloy-X is used in the combustion zone of gas turbine components such as transition ducts, combustor cans etc. The composition of the as-received alloy was tested from (Optical emission spectrometry) 'SpectraMax 130779' at Quality Test Laboratory, Mumbai, India is shown as in Table 1. The as-received plate is cut to 260 mm × 22 mm × 10 mm for machining the slot which was programmed. The alloy was solution heat-treated at 2150°F (1177°C) and rapidly cooled as established from the literature.[22]

### Experimental strategy

All the profile or shape that have to be machined was modelled and simulated in CNC software called ELCAM. In the current case, a circular profile with dimensions shown in Figure 1 was cut. The profile was converted into .WC code based on ELCAM software and this becomes the input to the Electronica 'ELPLUS 15 CNC WEDM'. It controls the wire guide movement and machining conditions for cutting based on the NC coding. A zinc-coated copper wire of 0.25 mm diameter and deionized water was used as dielectric fluid throughout the experiment. Figure 1(a) shows the slant type taper fixture where the workpiece is fixed to the WEDM table. This slant fixture made of aluminium H9 series by CNC. The workpiece Hastelloy-X is placed on the rotational angular plate. This plate can be locked to a specific angle based on the holes of the side plate as in Figure 1(b). It also shows the machined angular workpieces in orthogonal view obtained for three taper angles namely 0°, 15° and 30°.

**Table 1.** Chemical composition of Hastelloy-X.

| % | C% | Si% | Mn% | P% | S% | Cr% | Mo% | Fe% | Co% | W% | Ni% |
|---|---|---|---|---|---|---|---|---|---|---|---|
| Composition | 0.06 | 0.21 | 0.65 | 0.027 | 0.01 | 20.65 | 8.24 | 18.05 | 0.69 | 0.29 | 50.88 |
| Required composition | 0.05–0.15 | <1 | <1 | <0.04 | <0.03 | 20.5–23.0 | 8–10 | 17–20 | 0.5–2.5 | 0.2–1 | 50–60 |

### Characterization methodology

The profiling speed was calculated as the average of all speeds recorded at every instant during circular profiling from the WEDM. The surface roughness was measured using 'Mitutoyo SJ-301' surface roughness tester and an average of 5 values were calculated for analysis. The recast layer thickness was obtained from 'JEO JSM-6368OLA' and 'Hitachi SU 3500' scanning electron microscope (SEM) at 500X and 1000X magnification respectively. The SEM images with image J software and coordinate measuring machine (CMM) of 'TESA VISIO 200' make is used to measure the circular areas of 1 mm, 3 mm, 5 mm taper profiles. The 'OMNI TECH MVHS-AUTO' Vicker's micro-hardness tester was employed for micro-hardness where the micro-hardness of the base metal is 212Hv. ANN and ANFIS were modelled to predict the cutting speed using MATLAB software. ANFIS also provided a way to map the relationship between profiling speed and input parameter.

### Machining parameters

The parameters like pulse on time, pulse off time, servo feed and wire feed were kept constant throughout the study as shown in Table 2. These parameters were chosen based on the initial experiments on the workpiece and tool combinations.[12,13] Table 2 indicates the profiling parameters like $\vartheta$, $\mu$, $\varphi$ and $\omega$ that employed during slant profiling. These parameters were chosen based on the machining capability and initial experiments in Ref.[24] Based on initial experiments having minimal vibration and as based on slant type fixture height the $\vartheta$ parameters. The $\vartheta$ parameters were chosen as (40-70) for 0°, (75-105) for 15° and (100-130) for 30°. For 15° and 30° taper angle, the $\vartheta$ parameter will be different because of the tilting of the workpiece. As there were four factors and four levels $L_{16}$ Taguchi's orthogonal array was used for the investigation.

## Results and discussion

### Effect of machining parameters on profiling speed

The plots in Figure 2 show the variation of cutting speed at different parameters. It can be noticed that there is no significant effect of the $\vartheta$, $\mu$, $\varphi$ parameters on the profiling speed. From the effects plot, the $\omega$ parameter significantly controls the profiling speed during machining. There can be observed minor variations in profiling speed as in Figure 2 for $\vartheta$, $\mu$, $\varphi$

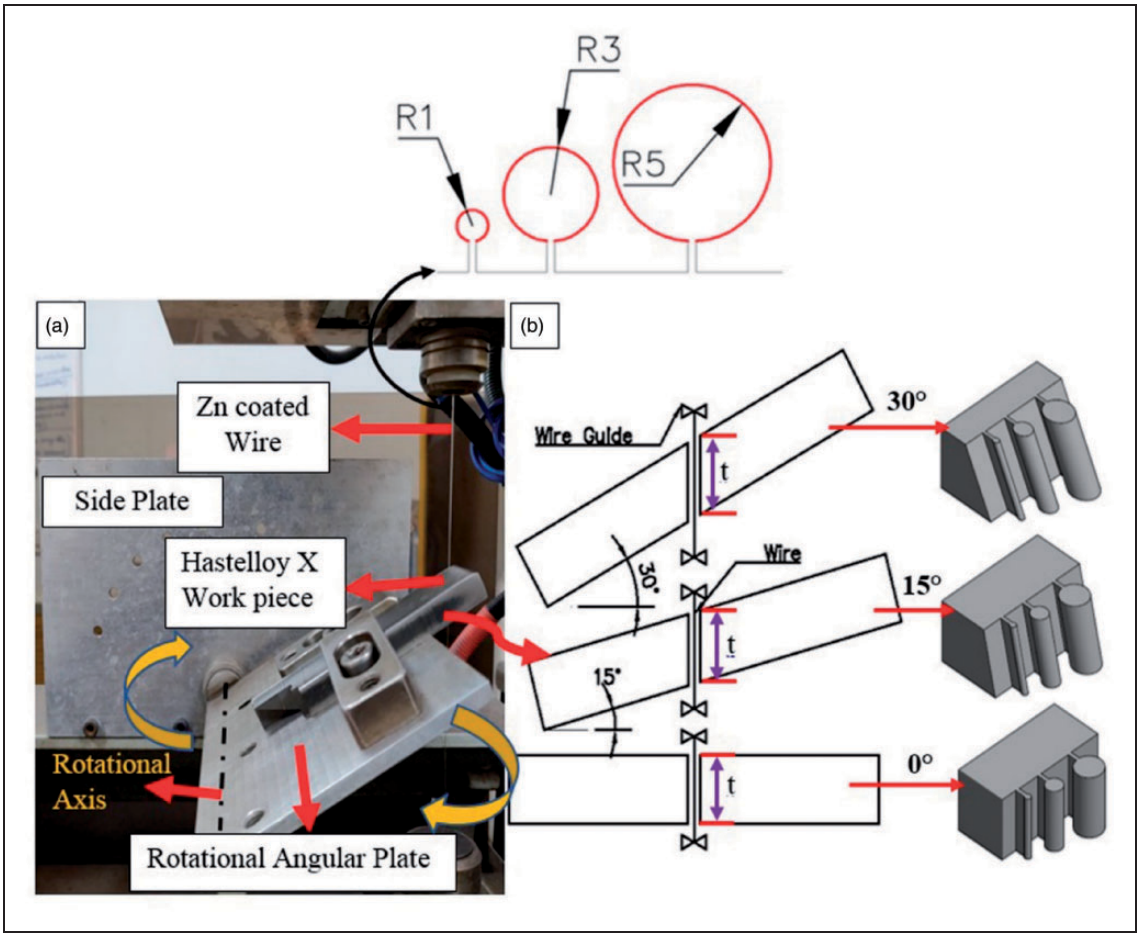


**Figure 1.** (a) Slant type taper fixture on WEDM table, (b) workpiece position at a different angle.

**Table 2.** WEDM parameters.

| | | | | | |
|---|---|---|---|---|---|
| Constant parameters | | | | | |
| EDM parameters | | Settings | | | |
| Pulse off time (μs) | | 44 | | | |
| Servo feed (mm/min) | | 20 | | | |
| Wire feed (m/min) | | 6 | | | |
| Pulse on time (μs) | | 115 | | | |
| Servo voltage (V) | | 40 | | | |
| Pulse current (A) | | 12 | | | |
| Flushing pressure (kg/cm$^2$) | | 0 (low pressure)[23] | | | |
| Corner control (%) | | 3[23] | | | |
| Radius compensation factor (microns) | | 0 ( for taper and complex profiles)[23] | | | |
| Profiling parameters | | | | | |
| Wire guide distance (mm) ($\vartheta$) | 0° | 40 | 50 | 60 | 70 |
| | 15° | 75 | 85 | 95 | 105 |
| | 30° | 100 | 110 | 120 | 130 |
| Cutting speed override (%)($\omega$) | | 31 | 54 | 77 | 100 |
| Wire offset (μm) ($\varphi$) | | 0 | 40 | 80 | 120 |
| Corner dwell time (s) ($\mu$) | | 0 | 33 | 66 | 99 |

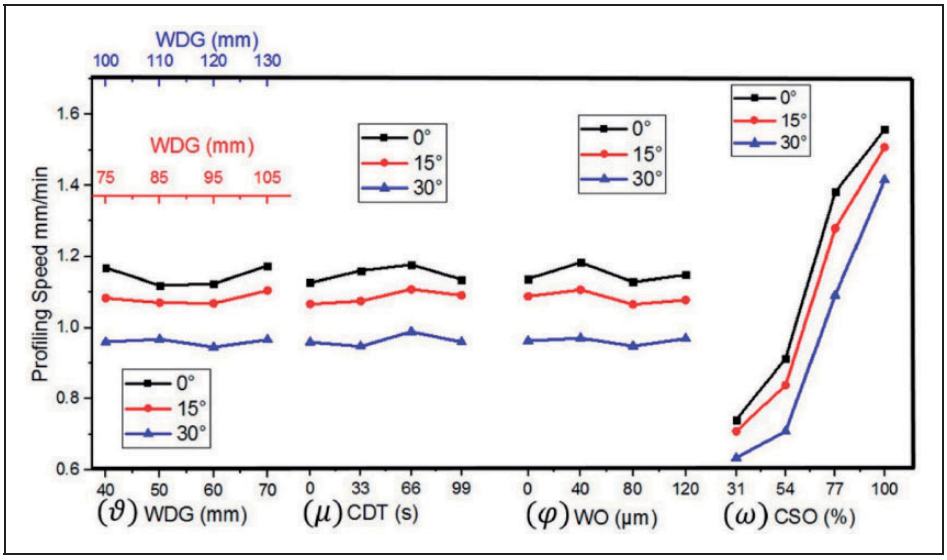


**Figure 2.** Variation of profiling speed at different machining parameters.

parameters. These variations were due to the machining errors during slant type taper profiling. The $\omega$ parameter is used during profiling for machining complex shape/profiles by controlling the required speed of machining.[23,24] It can be seen from Figure 2 that as the percentage of $\omega$ parameter increases the profiling speed also increases. There were small variations in the increase observed from Figure 2(d) at 54% and 77%. This phenomenon was due to the effect of vibrations during sparking and discharging.[12,25] The highest profiling speed recorded were 1.677 mm/min, 1.602 mm/min, and 1.457 mm/min and the lowest profiling speed of 0.718 mm/min, 0.701 mm/min, and 0.601 mm/min at respective taper angles. It can be observed from the plots that the 0° taper angle has the highest profiling speed and 30° taper angle has the lowest profiling speed. As the taper angle increased the profiling speed decreases due to the increase in the material cutting thickness.[24]

## *Effect of machining parameters on surface roughness*

Figure 3 shows the variation of surface roughness at various parameters for different taper angles and Table 3 shows the analysis of variance for surface roughness. It can be noticed that the $\mu$ parameter doesn't affect the surface roughness. The $\mu$ parameter mainly contributes to corner formations while machining complex profiles. It is a parameter that helps in recovery of wire lag due to the flexible nature of wire and in turn, it helps in the creation of sharp corners.[23] There are small variations that can be observed in Figure 3 this was due to the

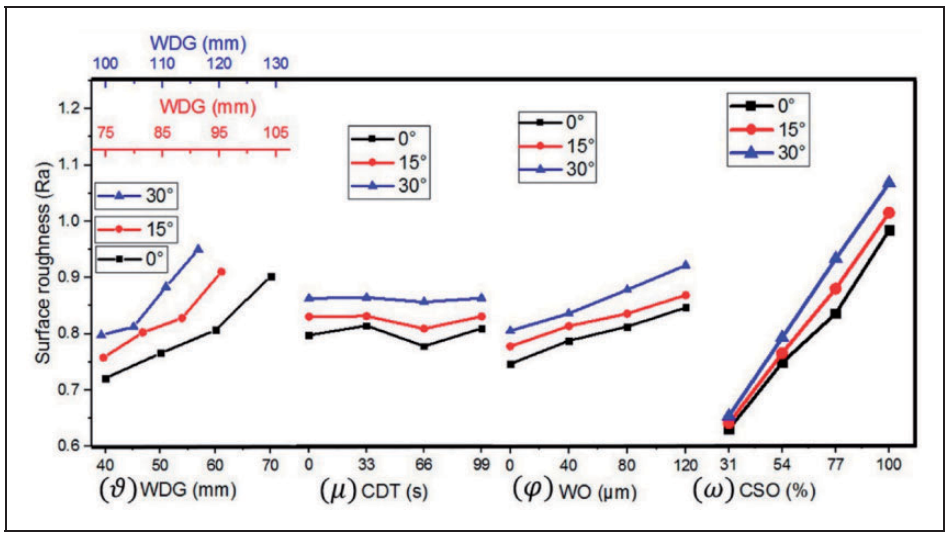


**Figure 3.** Variation of surface roughness at different machining parameters.

**Table 3.** Analysis of variance for surface roughness.

| Sl. No. | Factor | DF | Adj SS | Adj MS | F-Value | P-Value | % Contribution |
|---|---|---|---|---|---|---|---|
| **0°** | | | | | | | |
| 1 | $\vartheta$ | 3 | 0.022012 | 0.007337 | 1.39 | 0.396 | 8.55 |
| 2 | $\mu$ | 3 | 0.001909 | 0.000636 | 0.12 | 0.942 | 0.74 |
| 3 | $\varphi$ | 3 | 0.003190 | 0.001063 | 0.20 | 0.889 | 1.24 |
| **4** | $\boldsymbol{\omega}$ | **3** | **0.214585** | **0.071528** | **13.57** | **0.030** | **83.33** |
| 5 | Error | 3 | 0.015809 | 0.005270 | | | |
| 6 | Total | 15 | 0.257505 | | | | |
| **15°** | | | | | | | |
| 1 | $\vartheta$ | 3 | 0.022257 | 0.007419 | 0.86 | 0.548 | 7.78 |
| 2 | $\mu$ | 3 | 0.000798 | 0.000266 | 0.03 | 0.991 | 0.28 |
| 3 | $\varphi$ | 3 | 0.004703 | 0.001568 | 0.18 | 0.903 | 1.64 |
| **4** | $\boldsymbol{\omega}$ | **3** | **0.232251** | **0.077417** | **8.96** | **0.049** | **81.23** |
| 5 | Error | 3 | 0.025925 | 0.008642 | | | |
| 6 | Total | 15 | 0.285933 | | | | |
| **30°** | | | | | | | |
| 1 | $\vartheta$ | 3 | 0.020715 | 0.006905 | 0.79 | 0.574 | 6.88 |
| 2 | $\mu$ | 3 | 0.000174 | 0.000058 | 0.01 | 0.999 | 0.06 |
| 3 | $\varphi$ | 3 | 0.004632 | 0.001544 | 0.18 | 0.906 | 1.54 |
| **4** | $\boldsymbol{\omega}$ | **3** | **0.249377** | **0.083126** | **9.53** | **0.048** | **82.83** |
| 5 | Error | 3 | 0.026169 | 0.008723 | | | |
| 6 | Total | 15 | 0.301067 | | | | |

The parameters in bold are the most significant and highest contributing factor.

machining errors during profiling. It was also found that the surface roughness for 30° taper angle was always the highest compared to other angles. It is shown from Table 3 the $\omega$ parameter was the most significant compared to other input parameters.

The $\omega$ parameter is an online override parameter. This parameter is used for complex profiling, taper profiling and corner formation. It varies the profiling speed so that the machining can be carried out efficiently. As it is an override parameter it can modify the profiling speed regardless of machining parameters.[23] It can be seen in Figure 3 that as the percentage $\omega$ increases the surface roughness also increases. As the percentage $\omega$ increases, the discharge also upsurges having higher profiling speeds. This increases the sparks striking the workpiece during profiling. Due to the increase in the number of sparks the formation of craters, micro globules, modules, holes and metal debris, cracks etc. on the machined surface also escalates.[23,24] This leads to an increase in surface roughness at the machined surface. There were small variations at 77% of $\omega$ that can be observed in all the taper angles. These small variations in the increase were because of the wire vibrations during profiling.[25,26]

The $\vartheta$ parameter was the next important parameter with 6.88–8.55% contributing to surface roughness. The surface roughness increased in all the

taper angles as the $\vartheta$ parameter increased as shown in Figure 3. As the wire guide distance/wire span increases the distance between the guides also increases. Due to the increase in the length of the wire the tension of the wire decreases. This increases the wire vibration at the time of sparking. The wire vibration during profiling influences the sparking leading to the surface having higher surface roughness as observed by Chaudhary et al.[26] In Figure 3 to that as the $\vartheta$ increases, the surface roughness also increases gradually. There can be a small variation seen in 0° taper angle from 40 to 50 mm of $\vartheta$. These variations were due to the errors that were caused during the machining due to the changes in wire length. As wire length changed the tension also changes causing wire vibration.[25–27] This appeared to affect the surface roughness during machining.

The $\varphi$ was the next contributing factor and it indicates the wire offset given during profiling. Figure 3 shows as the $\varphi$ parameter increases the surfaces roughness of the profiles also escalates. The wire offset parameter is controlled during programming of profile. For higher values of wire offset the wire has to traverse larger than that of the programmed profile. This decreases the wire vibration which in turn increases the profiling speed as stated by Habib and Okada.[27] This increase in profiling speed causes an increase in sparking. As the sparking increases, the partially melted surface with peaks and valleys also increases. This escalates the surface roughness which was highlighted by Manoj et al.[12] Figure 3 shows a clear increase in the surface roughness but there were small variations at 80 μm of 0° taper angle. This phenomenon was noticed due to machining errors during profiling.

## *Effect of taper angle on profiling speed and surface roughness*

The tapered machine components of highest profiling speed parameters different angle were examined. It was found that as the taper angle increased the profiling speed decreased as shown in Figure 4. It also the surface roughness was recorded at both 0° and 30° taper angles. It can be noticed that as the taper increases the surface roughness increases which is contrasting to profiling speed. The profiling speed decreases as the taper increases because of the increase in material thickness. For the highest profiling parameter, even though the discharge energy remains constant the material thickness to cut increases with increase in the taper. This increases the time required to machine the workpiece decreasing the profiling speed.[24] In case of the surface roughness, the Figure 4(a) and (b) shows the SEM image of WEDMed surface at (a) 0° and (b) 30° taper angles respectively. It can be seen that in Figure 4(b) a larger number of smaller micro globules, modules, holes etc. As at 30° taper the machining the material thickness is higher, the melted material cannot be flush properly and re-solidifies on the machined surface due to the rapid cooling by the dielectric.[28] This increases the peak and valleys escalating the surface roughness. Contrastingly in case of 0° taper due to lower thickness and as the melted material was easily flushed with lower peak and valleys. This can also be seen in Figure 4(a) with lesser craters, micro globules, modules, holes etc. This decreases the surface roughness as shown in Figure 3 at lower taper angles. This effect is seen at different angles for almost the same cutting parameter only the change in taper angle leads to an increase in surface roughness. This result serves as a validation to the increase in surface roughness at higher taper angles as quoted in 'Effect of machining parameters on surface roughness' section.

## *Effect of machining parameters on circular profile areas*

It can be noticed from Table 4 that as the $\varphi$ parameter influences the most on the circular areas during taper profiling. It can be seen that the $\mu$ parameter have no or very small contribution to the circular areas. This is because $\mu$ parameter mainly focuses on the complex shapes and its formation during taper profiling. The $\mu$ parameter stops the wire at certain co-ordinate and gives time for the wire to travel towards the required co-ordinates reducing the wire lag.[23] The major significant parameter was $\varphi$ parameter.

The $\varphi$ is an offset parameter which increases the overall profile area by a fixed perpendicular distance. This parameter can be changed in NC programming and it was varied from 0–120 μm. As the $\varphi$ increases, the wire moves a fixed distance outside the programmed profile. This makes the wire to cut larger profiles compared to the programmed profiles. As the $\varphi$ parameter increases the profile area also increases with certain offset distance.[23,29] As $\varphi$ increases, the wire has to travel lager circumference compared to the programmed profile which increases the wire vibrations.[25,27,29] This leads to small variations in the increase as seen at 40μm for 0°, 15° and 30° of 1 mm taper profiles. With the increase in $\varphi$ parameter, the circular area also increases as shown in Figure 5 (a) this can be seen in all the taper angles. The $\varphi$ parameter is greatest contributing (64.42–72.92%) no the circular areas as shown in Table 4.

The $\vartheta$ parameter was the next significant parameter with the contributing factor with 19.09–24.38% as shown in Table 4. This controls the wire span/wire length between guides during machining. This parameter is mainly used while machining complex profiles, tapering and variable job thickness. As this parameter increases the wire span used for machining also increases.[23] With the increase in $\vartheta$ parameter, the wire lag and wire vibration escalate because of the tension in the wire decreases at higher spans.[29]

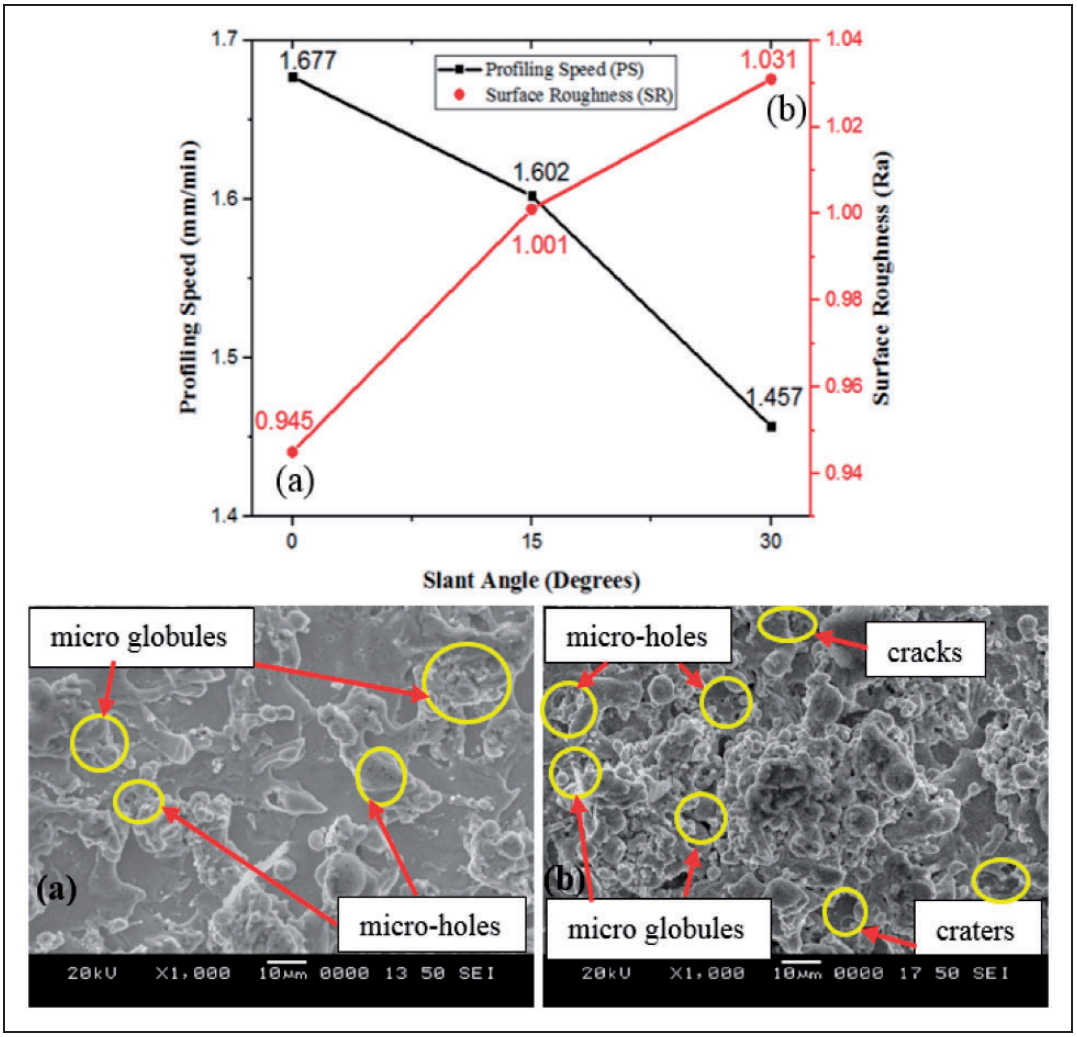


**Figure 4.** Variation of surface roughness and SEM images of WEDMed surface at (a) 0° and (b) 30° taper angles.

**Table 4.** ANOVA of circular areas at different angles.

| | | | 1mm areas | | 5mm areas | |
|---|---|---|---|---|---|---|
| Sl. no. | Factor | DF | Sum of squares | % contribution | Sum of squares | % contribution |
| **0°** | | | | | | |
| 1 | $\vartheta$ | 3 | 0.182 | 18.440 | 7.576 | 19.095 |
| 2 | $\mu$ | 3 | 0.010 | 1.034 | 0.411 | 1.035 |
| **3** | $\phi$ | **3** | **0.725** | **73.381** | **28.933** | **72.919** |
| 4 | $\omega$ | 3 | 0.042 | 4.235 | 2.010 | 5.066 |
| 5 | Error | 3 | 0.029 | 2.910 | 0.748 | 1.886 |
| **15°** | | | | | | |
| 1 | $\vartheta$ | 3 | 0.264 | 22.783 | 10.059 | 24.381 |
| 2 | $\mu$ | 3 | 0.005 | 0.463 | 0.101 | 0.245 |
| **3** | $\phi$ | **3** | **0.750** | **64.797** | **28.470** | **69.003** |
| 4 | $\omega$ | 3 | 0.115 | 9.914 | 1.907 | 4.622 |
| 5 | Error | 3 | 0.024 | 2.044 | 0.722 | 1.749 |
| **30°** | | | | | | |
| 1 | $\vartheta$ | 3 | 0.444 | 32.524 | 8.604 | 23.357 |
| 2 | $\mu$ | 3 | 0.009 | 0.624 | 0.126 | 0.343 |
| **3** | $\phi$ | **3** | **0.798** | **58.489** | **23.729** | **64.420** |
| 4 | $\omega$ | 3 | 0.077 | 5.645 | 3.014 | 8.183 |
| 5 | Error | 3 | 0.037 | 2.717 | 1.362 | 3.697 |

The parameters in bold highlight that it was the highest contributing factor among other parameters.

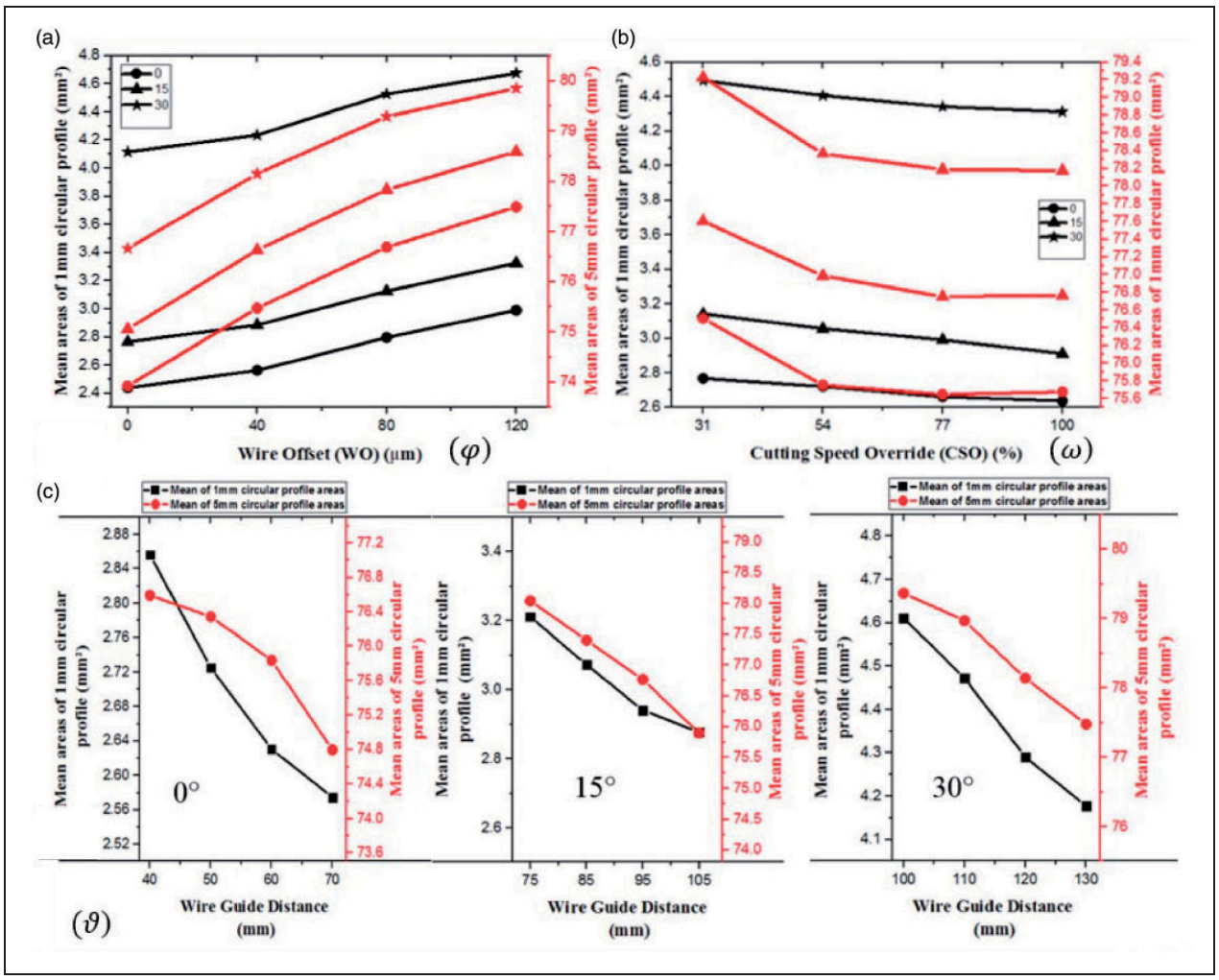


**Figure 5.** Variation of circular profile area for different machining parameters.

This phenomenon during machining decreases the circular area due to wire lag. The Figure 5(c) shows a clear decrease in circular areas as $\vartheta$ parameter escalates. There were small variations in decrease at 40 mm, 105 mm and 110 mm at respective taper angles due to vibrations in the wire. As the wire tension decreases the wire vibrates due to sparking also increases.[25,26]

The $\omega$ parameter was the next contributing factor and it was the most influential parameter on profiling speed as noticed in 'Effect of machining parameters on profiling speed' section. It is an on-line parameter that reduces or increases the profiling speed without modifying the set machining parameters. This parameter is used for machining complex profiles, taper profiles, and sharper corners. As % $\omega$ increases the machine varies the profiling speed depending on the region programmed profile like corner, curvature or straight cut. This parameter controls the cutting speed as it can alter the discharge energy irrespective of machining parameters.[23,24] As % $\omega$ increases the profiling speed escalates and the circular area decrease as shown in Figure 5(b). This implies that as the profiling speed increases, the area of circular profile decreases due to rapid travel of wire along the profile path. The wire lag increases with increase in profiling speed. This also increases the wire vibration due to the increase in discharge.[25,27] So it can be observed that vibrations are leading to small variation as in 77–100% of $\omega$ for 1 mm circular area. It was witnessed that after certain $\omega$ % or profiling speed the area tends to remain constant as highlighted by Sanchez et al.[30]

### *Variation of recast layer thickness, microhardness at different taper angles*

Figure 6 represents the recast layer of the taper circular profile at different angles for various profiling speeds. It can be noticed that the recast layer thickness decreases as the taper angle increases for both the highest and lowest profiling speed parameter. For higher taper angles, the workpiece is tilted or made slant. The wire has to machine slant thickness of the workpiece which increases with taper angle. With the increase in material thickness (slant thickness), better

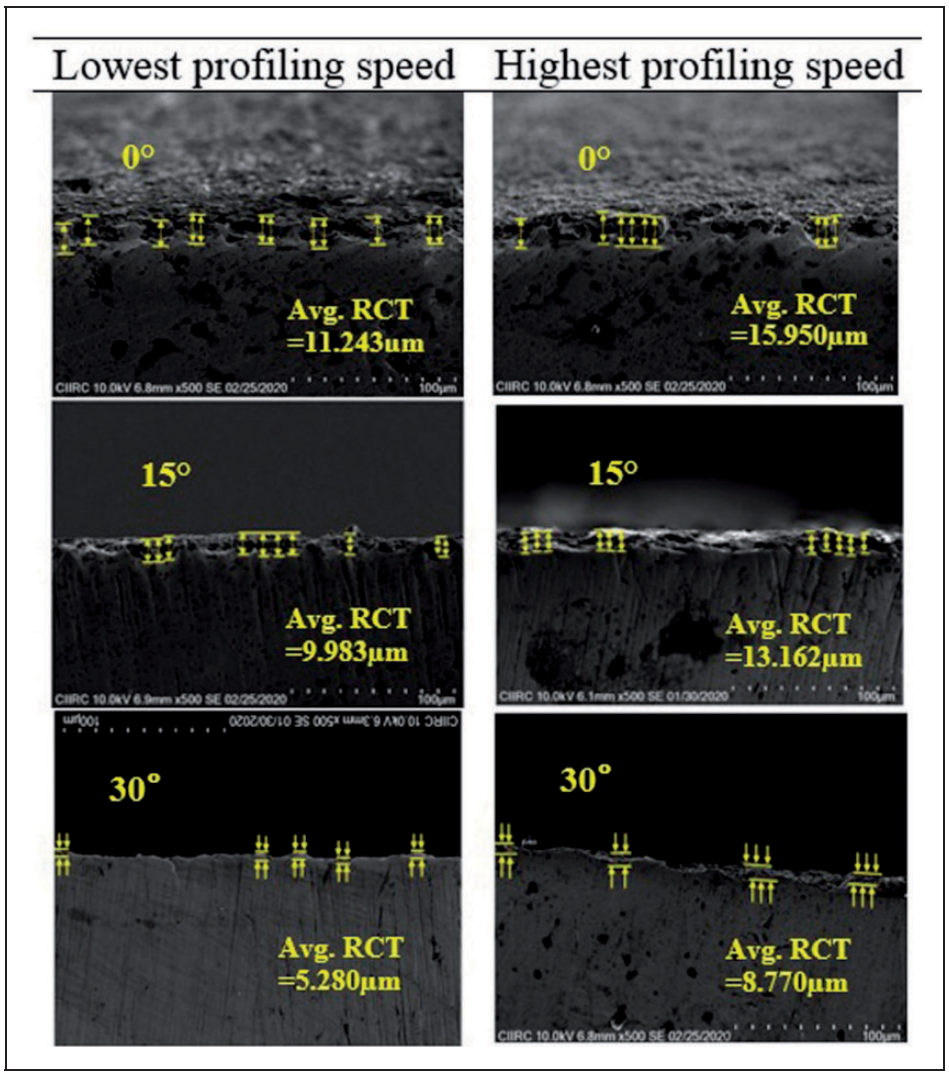


**Figure 6.** SEM images of the recast layer at different angles.

heat distribution and cooling of the surface occur for both cases of highest or lowest profiling parameter. So the recast layer thickness decreases for higher taper components. This also leads to a decrease in thermal degradation during machining for higher taper components.[13,31,32] It can be seen in Figure 7 that at higher taper angles for both the parameters the hardness of profile is more compared to 0° taper profiles. This WEDMed surface was subjected to EDS which indicates the diffusion of Cu, Zn and O as in Figure 8 form the zin coated copper wire. This makes the surface soft based on the amount of diffusion. Similar results were observed by Sharma et al.[33] in WEDM of Inconel.

## *ANN and ANFIS prediction of cutting speed at different slant angles*

The ANN and ANFIS models were modelled to the experiment carried at different parameters. There were 48 iterations of experiments conducted with 16 at each taper angle. Table 5 shows the details of the optimal model of both ANN and ANFIS. In the case of ANN modelling, all iterations were used for training, validation and testing for both the models. The data distribution made were 70% for training, 15% for validation and 15% for testing for ANN modelling. Backpropagation neural network (BPNN) with Levenberg-Marquardt (LM) algorithm as in Kara et al.[34,35] were utilized. For the neural network considered there are 1input layer, 1 hidden layer and 1output layer. The layers can be represented as[35]

$$U_i = f_1(W_{ij}X_i + b_{ij}) \tag{1}$$

Where, $i$=1, 2, 3, 4... and $j$=1, 2, 3, 4...[35]

$$Y_m = f_2(W_{km}V_k + b_{km}) \tag{2}$$

In the case of the ANFIS model, among 48 iterations of data 80% of the data was considered for training and validation the model and 10% were considered for the testing model. 5 network layers were employed in each network layer with 2 membership

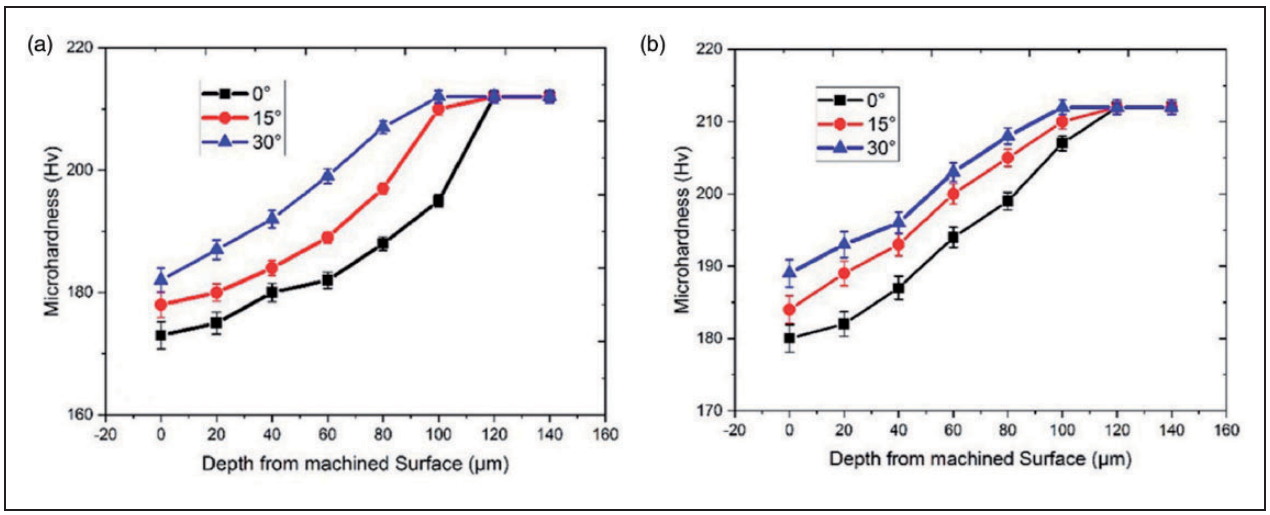


**Figure 7.** Microhardness at (a) highest and (b) lowest profiling parameters.

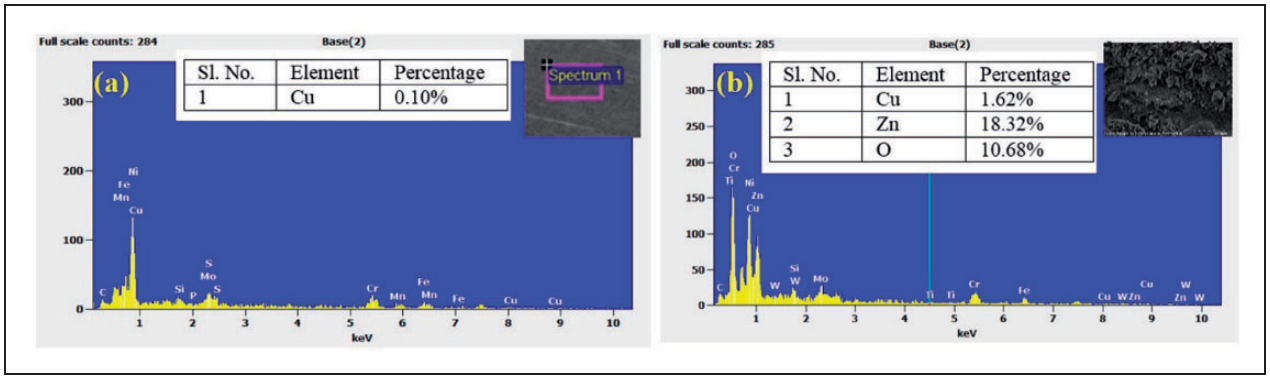


**Figure 8.** EDS of (a) as received and (b) WEDmed surface.

**Table 5.** Optimal model details.

| Sl. No. | Network parameters | Values |
|---|---|---|
| *Artificial neural network* | | |
| 1 | Network structure | 5-8-1-1 |
| 2 | Total number of training/validation/testing data sets | 32/8/8(48 experiments) |
| 3 | Network algorithm | Feed forward backpropagation |
| 4 | Type of transfer function | Tangential sigmoid |
| 5 | Type of training function | TRAINLM |
| 6 | Learning function | LEARNGDM |
| 7 | Performance function | MSE |
| *Adaptive neuro fuzzy interference system* | | |
| 1 | Total number of inputs | 48 |
| 2 | Total number of outputs | 1 |
| 3 | Total number of training/testing data sets | 38/10 |
| 4 | Type of input membership function | Gaussian |
| 5 | Type of output membership function | Constant |
| 6 | Total number of fuzzy rules | 32 rules |
| 7 | Number of epochs | 500/output |

function. The Gaussian membership function (gaussmf) was found optimal after many iterations and were utilized from the software toolbox as in Ref.[21,36] The system includes five inputs $x_1, x_2, x_3, x_4$ and $x_5$ the output $f_1$ and the rule base contains fuzzy rules which can be expressed by[37]

$$f_1 = p_1x_1 + q_1x_2 + r_1x_3 + l_1x_4 + x_5 \quad (3)$$

**Table 6.** Prediction of profile speed at various parameters for different taper angles.

| | | | | | | Profiling speed in mm/min (output) | | |
|---|---|---|---|---|---|---|---|---|
| Taper angle (degree) | Sl. No. | $\vartheta$ (mm) | $\mu$ (s) | $\varphi$ (μm) | $\omega$ (%) | ANN | ANFIS | Experimental |
| 0° | 1 | 40 | 0 | 0 | 31 | 0.765 | 0.756 | 0.756 |
| | 2 | 40 | 33 | 40 | 54 | 0.983 | 0.99 | 0.99 |
| | 3 | 40 | 66 | 80 | 77 | 1.394 | 1.309 | 1.392 |
| | 4 | 40 | 99 | 120 | 100 | 1.565 | 1.537 | 1.537 |
| | 5 | 50 | 0 | 40 | 77 | 1.334 | 1.337 | 1.337 |
| | 6 | 50 | 33 | 0 | 100 | 1.514 | 1.519 | 1.51 |
| | 7 | 50 | 66 | 120 | 31 | 0.745 | 0.748 | 0.748 |
| | 8 | 50 | 99 | 80 | 54 | 0.91 | 0.881 | 0.881 |
| | 9 | 60 | 0 | 80 | 100 | 1.5 | 1.502 | 1.501 |
| | 10 | 60 | 33 | 120 | 77 | 1.402 | 1.398 | 1.398 |
| | 11 | 60 | 66 | 0 | 54 | 0.881 | 0.879 | 0.879 |
| | 12 | 60 | 99 | 40 | 31 | 0.72 | 0.711 | 0.718 |
| | 13 | 70 | 0 | 120 | 54 | 0.862 | 0.898 | 0.898 |
| | 14 | 70 | 33 | 80 | 31 | 0.728 | 0.729 | 0.729 |
| | 15 | 70 | 66 | 40 | 100 | 1.679 | 1.677 | 1.677 |
| | 16 | 70 | 99 | 0 | 77 | 1.394 | 1.393 | 1.393 |
| 15° | 17 | 75 | 0 | 0 | 31 | 0.714 | 0.719 | 0.719 |
| | 18 | 75 | 33 | 40 | 54 | 0.855 | 0.85 | 0.85 |
| | 19 | 75 | 66 | 80 | 77 | 1.274 | 1.263 | 1.263 |
| | 20 | 75 | 99 | 120 | 100 | 1.512 | 1.502 | 1.501 |
| | 21 | 85 | 0 | 40 | 77 | 1.261 | 1.263 | 1.263 |
| | 22 | 85 | 33 | 0 | 100 | 1.464 | 1.468 | 1.468 |
| | 23 | 85 | 66 | 120 | 31 | 0.712 | 0.712 | 0.712 |
| | 24 | 85 | 99 | 80 | 54 | 0.831 | 0.838 | 0.838 |
| | 25 | 95 | 0 | 80 | 100 | 1.47 | 1.456 | 1.456 |
| | 26 | 95 | 33 | 120 | 77 | 1.276 | 1.274 | 1.274 |
| | 27 | 95 | 66 | 0 | 54 | 0.856 | 0.835 | 0.843 |
| | 28 | 95 | 99 | 40 | 31 | 0.697 | 0.701 | 0.701 |
| | 29 | 105 | 0 | 120 | 54 | 0.804 | 0.814 | 0.813 |
| | 30 | 105 | 33 | 80 | 31 | 0.694 | 0.693 | 0.693 |
| | 31 | 105 | 66 | 40 | 100 | 1.606 | 1.602 | 1.602 |
| | 32 | 105 | 99 | 0 | 77 | 1.3 | 1.298 | 1.311 |
| 30° | 33 | 100 | 0 | 0 | 31 | 0.622 | 0.619 | 0.62 |
| | 34 | 100 | 33 | 40 | 54 | 0.641 | 0.703 | 0.703 |
| | 35 | 100 | 66 | 80 | 77 | 1.113 | 1.106 | 1.106 |
| | 36 | 100 | 99 | 120 | 100 | 1.41 | 1.411 | 1.411 |
| | 37 | 110 | 0 | 40 | 77 | 1.09 | 1.089 | 1.089 |
| | 38 | 110 | 33 | 0 | 100 | 1.383 | 1.313 | 1.383 |
| | 39 | 110 | 66 | 120 | 31 | 0.677 | 0.682 | 0.682 |
| | 40 | 110 | 99 | 80 | 54 | 0.72 | 0.718 | 0.718 |
| | 41 | 120 | 0 | 80 | 100 | 1.402 | 1.405 | 1.405 |
| | 42 | 120 | 33 | 120 | 77 | 1.074 | 1.074 | 1.074 |
| | 43 | 120 | 66 | 0 | 54 | 0.691 | 0.701 | 0.696 |
| | 44 | 120 | 99 | 40 | 31 | 0.608 | 0.607 | 0.607 |
| | 45 | 130 | 0 | 120 | 54 | 0.714 | 0.708 | 0.708 |
| | 46 | 130 | 33 | 80 | 31 | 0.577 | 0.624 | 0.614 |
| | 47 | 130 | 66 | 40 | 100 | 1.447 | 1.457 | 1.457 |
| | 48 | 130 | 99 | 0 | 77 | 1.09 | 1.089 | 1.088 |

and so on. Where $p_i$, $q_i$, $r_i$ and $l_i$ are the linear parameters in the consequent part of the Sugeno fuzzy inference system. $i$=1, 2, 3, 4… and $j$=1, 2, 3, 4…[37]

$$Q_i = \sum_i \bar{w}_i f_i = \frac{\sum_i w_i f_i}{\sum_i w_i} \tag{4}$$

## *Validation of the optimal model*

Tables 6 and 7 show the ANN, ANFIS and experimental profiling speeds with validation experiments proving that the ANFIS was more accurate than the ANN model. The parameters for the validation experiments were chosen randomly and both ANN and ANFIS errors were indicated in Table 7. It was

**Table 7.** Validation of profiling speed at various parameters for different taper angles.

| | | | | | | Profiling speed in mm/min | | | | |
|---|---|---|---|---|---|---|---|---|---|---|
| Sl. no. | WDG (mm) | CDT (s) | WO (μm) | CSO (%) | Slant angle (degree) | Measured | ANN predicted | Error% | ANFIS predicted | Error% |
| 1 | 55 | 40 | 100 | 45 | 0° | 0.82 | 0.752 | 9.04 | 0.853 | 3.87 |
| 2 | 65 | 55 | 80 | 55 | 0° | 0.96 | 0.937 | 2.47 | 0.976 | 1.64 |
| 3 | 90 | 50 | 75 | 65 | 15° | 1.09 | 1.170 | 6.83 | 1.059 | 2.93 |
| 4 | 80 | 70 | 55 | 95 | 15° | 1.52 | 1.562 | 2.68 | 1.502 | 1.20 |
| 5 | 115 | 80 | 50 | 90 | 30° | 1.35 | 1.351 | 0.11 | 1.323 | 2.04 |
| 6 | 125 | 40 | 30 | 80 | 30° | 1.21 | 1.106 | 9.37 | 1.158 | 4.49 |

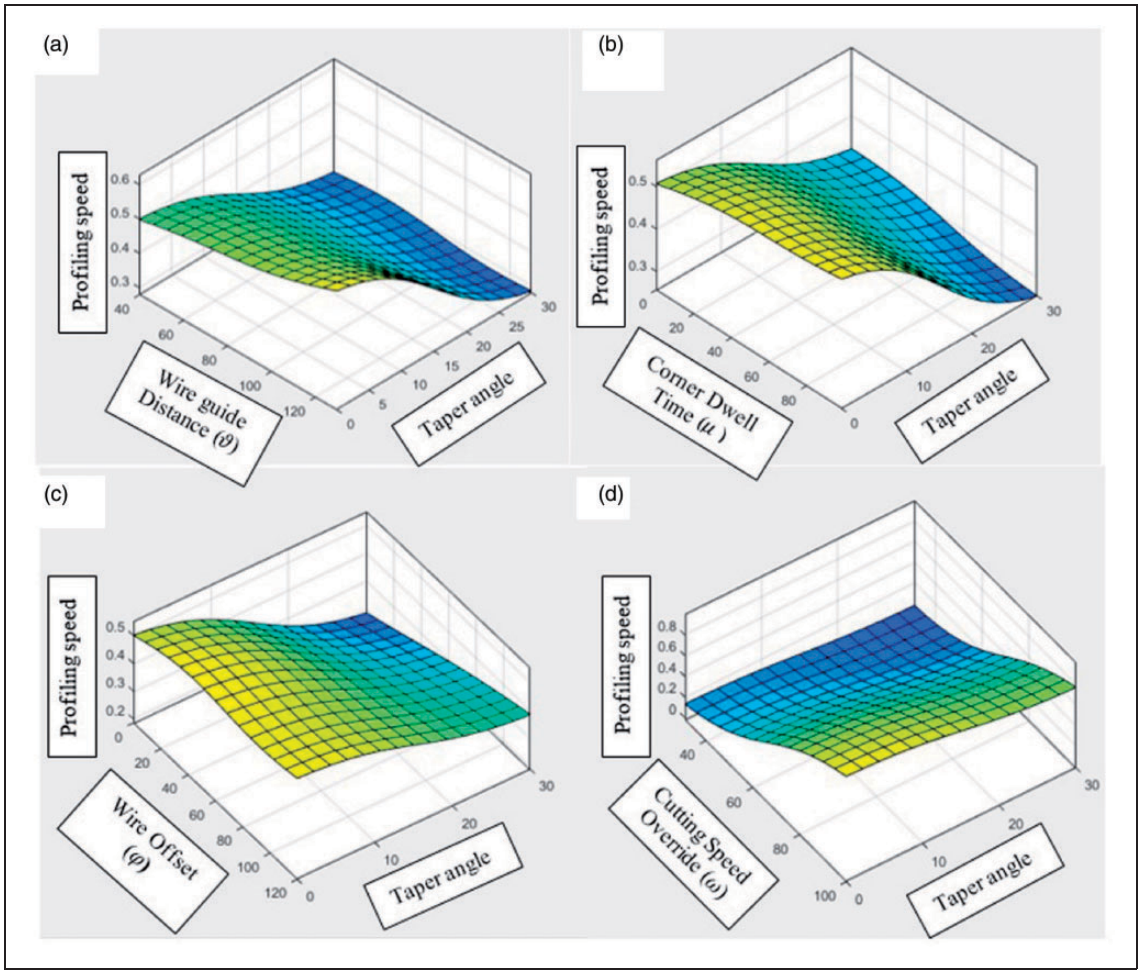


**Figure 9.** ANFIS mapping of profiling speed.

seen the ANFIS is better than ANN as percentage error range for ANFIS varied from 0–5% and ANN varied from 0–10%. Figure 9 showed the input-output mapping obtained from the ANFIS model. It can be observed that the profiling speed decreases with increasing taper angle as highlighted in 'Effect of taper angle on profiling speed and surface roughness' section. It can also be witnessed that $\vartheta$ and $\varphi$ also contribute to the profiling speed which couldn't be highlighted in effects plot in 'Effect of machining parameters on profiling speed' section. The Figure 9(a) and (d) shows the variation of $\vartheta$ and $\varphi$. It can be observed that as $\vartheta$ increases the profiling speed slightly increases. In the case of $\varphi$, there is slightly decrease of profiling speed with increase in $\varphi$ parameter as highlighted by Habib and Okada.[27]

## Conclusion

The tapering has been achieved overcoming disadvantages of the conventional method in WEDM using slant type taper fixture. The variation

of response parameters were highlighted after machining a circular profile on Hastelloy-X. From the above study different the following inference can be outlined.

1. The $\omega$ parameter majorly influences the profiling speed and surface roughness. As the $\omega$ parameter increases, there is an increase in cutting speed from 110.10% to 124.20% and a decrease in surface roughness from 56.32%-63.65%. This was due to the escalation in discharge as $\omega$ parameter increases.
2. In the case of circular profile areas, the $\varphi$ parameter mainly controlled the circular areas. As the $\varphi$ parameter increases circular area escalate to 4.7% to 22.22% because of the increase in offset distance of wire during profiling.
3. The recast layer thickness clearly shows a decrease from 53.25–45.02% and micro-hardness at WEDMed surface increases 5.13–5.813% as the taper angle increases from 0° to 30°. This was because of increased (slant material thickness) material thickness and a better distribution of heat.
4. In the case of prediction of profiling speed, the ANFIS clearly shows accuracy compared to ANN as the average error was less for ANFIS (0.44%) when compared to ANN (0.79%). ANFIS mapping also shows the relationship between input and output parameters.

## Declaration of Conflicting Interests

The author(s) declared no potential conflicts of interest with respect to the research, authorship, and/or publication of this article.

## Funding

The author(s) received no financial support for the research, authorship, and/or publication of this article.

## ORCID iD

IV Manoj https://orcid.org/0000-0003-1556-3896

## References

1. Aggarwal V, Pruncu CI, Singh J, et al. Empirical investigations during WEDM of Ni-27Cu-3.15Al-2Fe-1.5Mn based superalloy for high temperature corrosion resistance applications. *Materials* 2020; 13: 3470.
2. Shandilya P, Rouniyar AK and Saikiran D. Multi-objective parametric optimization on machining of Inconel-825 using wire electrical discharge machining. *Proc IMechE, Part C: J Mechanical Engineering Science* 2020; 234: 5833–5847.
3. Thakur A and Gangopadhyay. State-of-the-art in surface integrity in machining of nickel based super alloys. *Int J Mach Tool Manuf* 2016; 100: 25–54.
4. Prakash C, Singh S, Pruncu CI, et al. Surface modification of Ti-6Al-4V alloy by electrical discharge coating process using partially sintered Ti-Nb electrode. *Materials* 2019; 12: 1006.
5. Venkatarao K and Anup Kumar T. An experimental parametric analysis on performance characteristics in wire electric discharge machining of Inconel 718. *Proc IMechE, Part C: J Mechanical Engineering Science* 2019; 233: 4836–4849.
6. Mouralova K, Prokes T and Benes L. Analysis of the oxide occurrence on WEDM surfaces in relation to subsequent surface treatments. *Proc IMechE, Part C: J Mechanical Engineering Science* 2019; 44: 7723–7735.
7. Plaza S, Ortega N, Sanchez JA, et al. Original models for the prediction of angular error in wire-EDM taper-cutting. *Int J Adv Manuf Technol* 2009; 44: 529–538.
8. Kinoshita N, Fukui M and Fujii, T. Study on wire-EDM: accuracy in taper-cut. *CIRP Ann Manuf Technol* 1987; 36: 119–122.
9. Sanchez JA, Plaza S, Lopez De Lacalle LN, et al. Computer simulation of wire-EDM taper-cutting. *Int J Comput Integ M* 2006; 19: 727–735. doi:10.1080/09511920600628855.
10. Yan H, Liu Z, Li L, et al. Large taper mechanism of HS-WEDM. *Int J Adv Manuf Technol* 2017; 90: 2969–2977.
11. Martowibowo SY and Wahyudi A. Taguchi method implementation in taper motion wire EDM process optimization. *J Ins Eng Ser C* 2012; 93: 357–364.
12. Manoj IV, Joy R and Narendranath S. Investigation on the effect of variation in cutting speeds and angle of cut during slant type taper cutting in WEDM of Hastelloy-X. *Arab J Sci Eng* 2020; 45: 641–651.
13. Joy R, Manoj IV and Narendranath S. Investigation of cutting speed, recast layer and micro-hardness in angular machining using slant type taper fixture by WEDM of Hastelloy-X. *Mater Today* 2020; 27: 1943–1946.
14. Gong YD, Sun Y, Wen XL, et al. Experimental study on accuracy and surface quality of TC2 in LS – WEDM multiple cuts. *J Braz Soc Mech Sci Eng* 2016; 38: 2421–2433.
15. Tahir W and Jahanzaib M. Multi-objective optimization of WEDM using cold treated brass wire for HSLA hardened steel. *J Braz Soc Mech Sci Eng* 2019; 41:525.
16. Khatri BC and Rathod PP. Investigations on the performance of concentric flow dry wire electric discharge machining (WEDM) for thin sheets of titanium alloy. *Int J Adv Manuf Technol* 2017; 92: 1945–1954.
17. Firouzabadi HA and Parvizian J. Improving accuracy of curved corners in wire EDM successive cutting. *Int J Adv Manuf Technol* 2015; 76: 447–459.
18. Dodun O, Gonçalves-Coelho AM, Slătineanu L, et al. Using wire electrical discharge machining for improved corner cutting accuracy of thin parts. *Int J Adv Manuf Technol* 2009; 41: 858–864.
19. Jafari R, Kahya M, Oliaei SNB, et al. Modeling and analysis of surface roughness of microchannels produced by $\mu$-WEDM using an ANN and Taguchi method. *J Mech Sci Technol* 2017; 31: 5447–5457.
20. Azhiri RB, Teimouri R, Baboly MG, et al. Application of Taguchi, ANFIS and grey relational analysis for studying, modeling and optimization of wire EDM process while using gaseous media. *Int J Adv Manuf Technol* 2014; 71: 279–295.
21. Naresh C, Bose PSC and Rao CSP. Artificial neural networks and adaptive neuro−fuzzy models for predicting WEDM machining responses of Nitinol alloy: comparative study. *SN Appl Sci* 2020; 2: 314.

22. Chandler H. *Heat Treater's guide practices and procedures for nonferrous alloys. Third printing* (2006). ASM International®, The Materials Information Society.
23. Electronica India Ltd. *Operating manual for ELPLUS 15 Ecocut*, 2011.
24. Manoj IV, Joy R, Narendranath S, et al. Investigation of machining parameters on corner accuracies for slant type taper triangle shaped profiles using WEDM on Hastelloy X. *IOP Conf Ser Mat Sci Eng* 2019; 591: 1–11.
25. Puri AB and Bhattacharyya B. Modelling and analysis of the wire-tool vibration in wire-cut EDM. *J Mater Process Technol* 2003; 141: 295–301. doi: 10.1016/S0924-0136(03)00280-2.
26. Chaudhary T, Siddiquee AN, Chanda AK. Effect of wire tension on different output responses during wire electric discharge machining on AISI 304 stainless steel. *Def Technol* 2016; 15: 541–544.
27. Habib S and Okada A. Experimental investigation on wire vibration during fine wire electrical discharge machining process. *Int J Adv Manuf Technol* 2016; 84: 2265–2276.
28. Goswami A and Kumar J. Trim cut machining and surface integrity analysis of Nimonic 80A alloyusing wire cut EDM. *Eng Sci Technol Int J* 2017; 20: 175–186.
29. Manoj IV and Narendranath S. Variation and artificial neural network prediction of profile areas during slant type taper profiling of triangle at different machining parameters on Hastelloy X by wire electric discharge machining. *Proc IMechE, Part E: J Process Mechanical Engineering* 2020; 234: 673–683.
30. Sanchez JA, Plaza S, Ortega N, et al. Experimental and numerical study of angular error in wire-EDM taper-cutting. *Int J Mach Tool Manuf* 2008; 48: 1420–1428.
31. Manjaiah M and Rudolph LF. Study on recast layer thickness and residual stress during WEDM of SMAs. *Emerg Mater Res* 2017; 6: 82–88.
32. Manjaiah M, Narendranath S, Basavarajappa S, et al. Effect of electrode material in wire electro discharge machining characteristics of Ti50Ni50−xCux shape memory alloy. *Precis Eng* 2015; 41: 68–77.
33. Sharma P, Chakradhar D and Narendranath S. Effect of wire material on productivity and surface integrity of WEDM-processed Inconel 706 for aircraft application. *J Mater Eng Perform* 2016; 25: 3672–3681.
34. Kara F, Aslantas K and Çiçek A. ANN and multiple regression method-based modelling of cutting forces in orthogonal machining of AISI 316L stainless steel. *Neural Comput Appl* 2014; 26: 237–250.
35. Kara F, Aslantas K and Çiçek A. Prediction of cutting temperature in orthogonal machining of AISI 316L using artificial neural network. *Appl Soft Comput* 2016; 38: 64–74.
36. Sharma VS, Sharma SK and Sharma AK. An approach for condition monitoring of a turning tool. *Proc IMechE, Part B: J Engineering Manufacture* 2007; 221: 635–648.
37. Tiwari S, Babbar R and Kaur G. Performance evaluation of two ANFIS models for predicting water quality index of river Satluj (India). *Adv Civ Eng* 2018; 1–10 (Article ID 8971079).

## Appendix

### Notation

| | |
|---|---|
| ANFIS | adaptive neuro-fuzzy interference system |
| ANN | artificial neural network |
| $b_{ij}$ | the biases of the 1st hidden layer |
| $b_{km}$ | biases of the output layer |
| CNC | computer numerically control |
| $f_i$ | fuzzy rules |
| $f_1$ | the tan-sig transfer function |
| $f_2$ | pure-line transfer function |
| $Q_i$ | overall output |
| SEM | scanning electron microscope |
| $U_i$ | the outputs of the 1st layer (input) |
| $V_k$ | input from the previous layer |
| WEDM | wire electric discharge machining |
| $\bar{w}_i$ | output of (layer 3) |
| $W_{ij}$ | the weights from the input layer |
| $W_{km}$ | weights from hidden layer k to output layer m |
| $X_i$ | the input of the input layer |
| $Y_m$ | outputs of the hidden layer |
| $\mu$ | corner dwell time (s) |
| $\omega$ | cutting speed override (%) |
| $\varphi$ | wire offset (μm) |
| $\vartheta$ | wire guide distance (mm) |